Insights into the Preparation of Supported Catalysts: A Spatially Resolved Raman and UV−Vis Spectroscopic Study into the Drying Process of CoMo/γ-Al_2O_3 Catalyst Bodies

Leon G. A. van de Water,[†] Jaap A. Bergwerff,[†] Bob (R.) G. Leliveld,[‡] Bert M. Weckhuysen,[†] and Krijn P. de Jong*[,†]

Department of Inorganic Chemistry and Catalysis, Debye Institute, Utrecht University, Sorbonnelaan 16 3508 TB Utrecht, The Netherlands, and Albemarle Catalysts BV, Nieuwendammerkade 1-3, 1022 AB Amsterdam, The Netherlands

Received: March 1, 2005; In Final Form: May 17, 2005

Spatially resolved Raman and UV−vis−NIR microspectroscopy have been used as tools to study the preparation process of supported catalyst bodies. Detailed spectroscopic information on the local coordination geometry of two different metallic species along with their macro-distribution over the catalyst body has been obtained, enabling a good understanding of the physicochemical processes occurring during the drying process of impregnated γ-Al_2O_3 bodies. The formation and decomposition of the Keggin-type complex $H_xPMo_{11}CoO_{40}^{(7-x)-}$, which is considered to be a potential precursor for $CoMoS_2$/γ-Al_2O_3 HDS catalysts, inside γ-Al_2O_3 bodies is shown to be a function of the composition of the impregnation solutions, the aging time, and the drying conditions applied. This knowledge has been successfully applied to prepare samples with a well-defined distribution of the bimetallic complex, that is, either egg-shell, egg-yolk, or homogeneous distributions. The Raman results are presented in a semiquantitative way by subtraction of a reference spectrum of a sample containing a known amount of $H_xPMo_{11}CoO_{40}^{(7-x)-}$ from the spectra recorded along the cross-section of the catalyst bodies.

Introduction

Heterogeneous catalysis plays a dominant role in a vast number of processes in modern society, for example, in the refining of oil, the manufacturing of chemicals, and in environmental catalysis.[1] Generally speaking, the preparation of a solid catalyst involves the impregnation of a catalyst support (which may be a powder or millimeter-sized shaped support bodies) with a solution containing a precursor species of the active component, followed by aging, drying, calcination, and, in some cases, treatments such as reduction, oxidation, or sulfidation. The activity of the resulting catalyst depends on the speciation of the active component along with its dispersion and macro-distribution throughout the support (body). For the systematic development of catalysts, controlling the (physical) chemistry from the nanometer level up to the millimeter level is desirable during all steps of the preparation process.[1b,2] Although the literature on catalyst preparation is extensive, many of the phenomena occurring during impregnation, aging, drying, and calcination still defy thorough understanding.[3]

An example of a heterogeneously catalyzed industrial process is the hydrodesulfurization (HDS) of fuels, for which sulfided cobalt/molybdenum, supported on γ-Al_2O_3, is generally employed. The catalytically active phase is believed to be a "CoMoS" phase, where Co is located on the edges of MoS_2 crystallites.[4] The preparation process involves impregnation of γ-Al_2O_3 support bodies with a Co- and Mo-containing aqueous solution, followed by aging, drying, calcination, and sulfidation. To obtain a good dispersion of both Co and Mo over the catalyst−support body after sulfidation, a homogeneous metal distribution throughout the whole preparation procedure is expected to be beneficial, although redistribution of the catalytically active species may occur upon calcination and sulfidation. Unfortunately, characterization studies dealing with the analysis of the metal speciation and distribution at the different stages of the preparation process are scarce.[5] Furthermore, samples in powder form are most often analyzed in these studies, whereas millimeter-sized support bodies are industrially much more relevant.

Simple Co and Mo salts such as cobalt nitrate and ammonium heptamolybdate (AHM, $[NH_4]_6Mo_7O_{24}$) are not the most suited precursors for the preparation of $CoMoS_2$/γ-Al_2O_3 catalysts, as reaction of the Co and Mo with the Al_2O_3 support may occur upon aging and drying, whereby $CoAl_2O_4$ ("surface spinel") species[6] and Anderson-type $[Al(OH)_6Mo_6O_{18}]^{3-}$ heteropolyanions,[7] respectively, are formed. This may result in nonhomogeneous Co and Mo distributions over the support body and, moreover, makes the Co unavailable for the sulfidation step. Impregnation with solutions of Mo- and Co-containing complex heteropolyanions (HPAs) has been proposed to improve the dispersion of the precursor species and reduce the reactivity with the support.[8] In this respect, Anderson-type heteropolyoxomolybdates (for example $[Co^{III}(OH)_6Mo_6O_{18}]^{3-}$ and phosphorus-containing Keggin-type HPAs[10] (see Figure 1) have been reported. $Co_{3/2}PMo_{12}O_{40}$, with Co^{2+} acting as the counterion for the P- and Mo-containing Keggin HPA, has the disadvantage that it decomposes upon impregnation due to the high pH that often prevails within the pores of the Al_2O_3 support. This results in surface polymolybdate species and $H_xPO_4^{(3-x)-}$, which reacts with the surface, yielding an $AlPO_4$-type surface phase.[11] The stability of the Keggin-type HPA can be improved by using

* Corresponding author. Phone: 0031-302537400. Fax: 0031-302511027. E-mail: k.p.deJong@chem.uu.nl.
[†] Utrecht University.
[‡] Albemarle Catalysts BV.

10.1021/jp051037e CCC: $30.25
Published on Web 07/13/2005

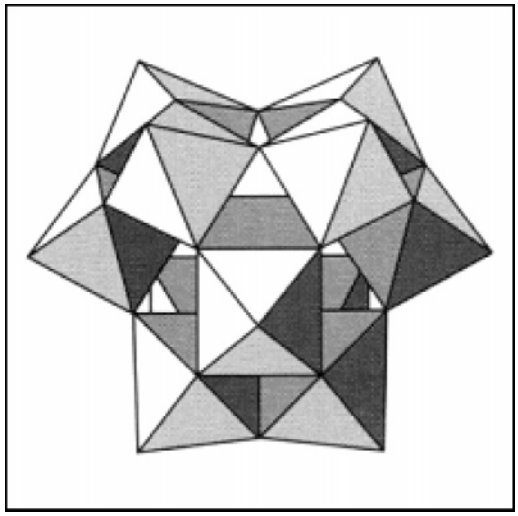

Figure 1. Schematic representation of a Keggin-type heteropolyanion with the general formula $[XY_{12}O_{40}]^{z-}$.

reduced HPA species, such as $Co_{7/2}PMo_{12}O_{40}$,[9c] or by applying organic solvents instead of water.[12]

We have chosen to use a precursor in which Mo and Co are present within the same Keggin-unit: $H_xPMo_{11}CoO_{40}^{(7-x)-}$ (abbreviated as $PMo_{11}Co$). Transition-metal-substituted HPAs are known to form easily from "lacunary" heteropolyanions, such as $H_xPMo_{11}O_{39}^{(7-x)-}$.[13] In an earlier paper, we have described the results of impregnation experiments involving solutions of $PMo_{11}Co$ and γ-Al_2O_3 pellets, where Raman and UV−vis−NIR (diffuse reflectance mode) microspectroscopy were applied to monitor and understand the evolution process of $PMo_{11}Co$ during impregnation.[14] Impregnation with PMo_{11}-Co-containing solutions appeared to result in fast decomposition of the HPA inside the γ-Al_2O_3 support.[14] In the search for precursor solutions that yield $PMo_{11}Co$ inside the support upon impregnation (and aging), solutions containing $[NH_4]_6Mo_7O_{24}$, $Co(NO_3)_2{\cdot}6H_2O$, citric acid, and varying amounts of H_3PO_4 were applied. It turned out that the $PMo_{11}Co$ complex may be formed inside the pores of the support upon aging, where the formation depends on the initial H_3PO_4 concentration in the impregnation solution and on the aging time.[14]

In this paper, we present the results of a spectroscopic study on the drying process of impregnated γ-Al_2O_3 pellets. The conditions under which $PMo_{11}Co$ can be observed inside the pellets after drying as well as the influence of the drying conditions on the distribution of this complex are dealt with. We show that by understanding the physical chemistry of the preparation process the final distribution of the catalyst precursor $PMo_{11}Co$ can be influenced in such a way that either a homogeneous, an egg-yolk or an egg-shell distribution can be obtained after drying. Spatially resolved UV−vis−NIR (diffuse reflectance mode)[15] and Raman[16] microspectroscopy are applied as the analytical tools that provide the information on both the Co and Mo distribution over the catalyst bodies and on their local coordination geometry. Furthermore, the Raman data have been used to present the data in a semiquantitative way by means of spectral subtraction using a reference spectrum with known $PMo_{11}Co$ concentration.

Experimental Section

In all experiments, cylindrical γ-Al_2O_3 pellets (Engelhard, 3 mm in both length and diameter) have been applied. These were calcined at 600 °C for 6 h and stored at 120 °C prior to impregnation. The pore volume of this support material was 1.0 mL/g, and its surface area was 200 m^2/g. Pore-volume impregnation was performed, the volume of the impregnation solution being equal to the pore volume of the γ-Al_2O_3 sample plus 10%. Impregnation solutions were prepared by adding a solution of citric acid (OPG Pharma, p.a.) and H_3PO_4 (85 wt % solution, Merck, p.a.) to a $[NH_4]_6Mo_7O_{24}$ (Acros, p.a.) solution. Finally, solid $Co(NO_3)_2{\cdot}6H_2O$ (Acros, p.a.) was added. Citric acid[16,17] and H_3PO_4[5b,16] are commonly used additives in impregnation solutions for CoMo/γ-Al_2O_3 catalysts due to their complexing ability toward Mo which is thought to enhance the dispersion of the metallic catalyst precursor species over the Al_2O_3 support. All solutions contained 1.0 M Mo, 0.5 M Co, 0.2 M citric acid, and H_3PO_4 in varying concentrations; they are abbreviated as CoMoCAP(x), with x being the H_3PO_4 molar concentration. Impregnated pellets were aged for either 4 or 24 h and subsequently dried in static air in a preheated oven at 120 °C (12 h) (fast drying) or by slowly heating the samples (1 °C/min) up to 120 °C and keeping them for 12 h at that temperature (slow drying). After cooling to room temperature, the pellets were analyzed by recording spatially resolved Raman and UV−vis−NIR spectra in a line through the middle of the cross-section of pellets that were bisected in the middle, perpendicular to their axis.

Raman spectra were recorded on these bisected pellets using a Kaiser RXN spectrometer equipped with a 785-nm diode laser in combination with a Hololab 5000 Raman microscope. A 10× objective was used for beam focusing and collection of scattered radiation, resulting in a spot size on the sample of approximately 50 μm. The laser output power was 70 mW. For a typical measurement, 5 spectra were accumulated with a 15-s exposure time. UV−vis−NIR spectra were recorded in much the same way using a specially designed setup for spatially resolved UV−vis−NIR measurements.[15] The spatial resolution of these measurements was around 100 μm, and 10−15 spectra were recorded along each cross-section.

Semiquantitative results were obtained by subtraction of the Raman spectrum of a $PMo_{11}Co$-containing reference sample from spectra containing multiple components. A reference spectrum with a maximum amount of all Mo present in the $PMo_{11}Co$ complex was obtained by a series of experiments with crushed γ-Al_2O_3 pellets (150−500-μm sieve fraction). These crushed pellets were impregnated with CoMoCAP(x) impregnation solutions, with x ranging from 0.3 to 2.0. After 4-h aging and fast drying, Raman spectra were recorded, and the spectrum of the sample with the largest $PMo_{11}Co$ content was chosen for the quantification. This spectrum (of the sample impregnated with the CoMoCAP(0.8) solution) appeared to be very similar to that of a solution with 88% of all Mo present in $PMo_{11}Co$, which was obtained from a titration experiment with varying H_3PO_4 concentrations.[14] (See also Results and Discussion section.) All spectra were subjected to baseline correction, and the height of the NO_3^- peak was used for scaling of the spectra. The NO_3^- peak has been proven to be suitable for scaling of spectra recorded on wet samples,[16] where it was found that a homogeneous NO_3^- distribution was obtained after 10 min. The NO_3^- distribution after drying of impregnated γ-Al_2O_3 pellets is still homogeneous, as no radial concentration gradient was observed after drying of γ-Al_2O_3 pellets that were impregnated with a 1.0 M NH_4NO_3 solution. The error in the semiquantitative results was estimated to be approximately 15%.

Attempts to use the UV−vis−NIR spectra for quantification of $PMo_{11}Co$ failed due to interference of the Co^{2+} $d-d$ band of $CoAl_2O_4$ (surface spinel) at 15750 cm^{-1} with the Co^{2+} $d-d$ band of $PMo_{11}Co$ at 17800 cm^{-1}. The lower-energy side of this

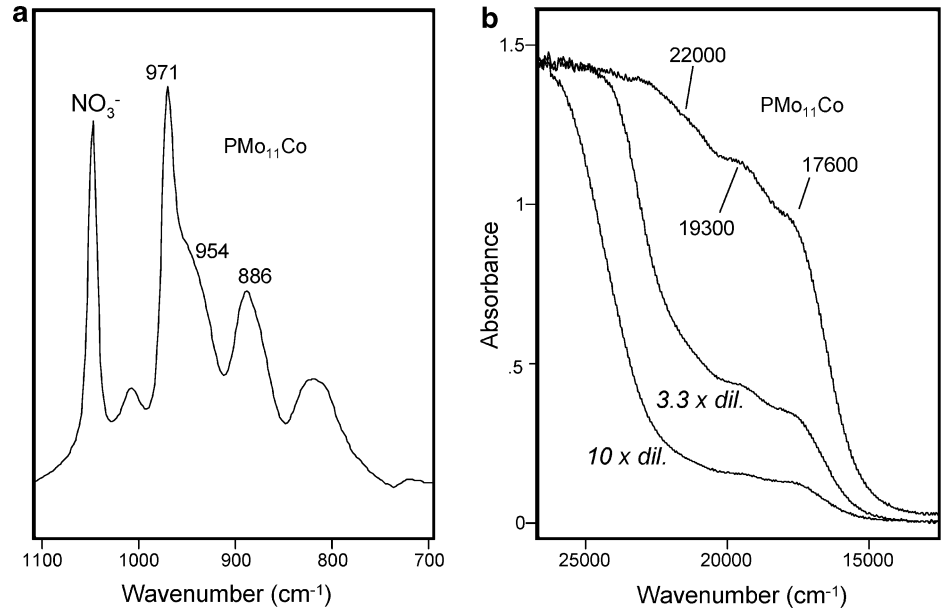

Figure 2. (a) Raman and (b) UV−vis−NIR spectra of the CoMoP(0.12) solution, containing 88% $PMo_{11}Co$. In (b), the spectra of diluted samples are depicted for clarity reasons.

band has been used previously for the quantification of impregnated wet samples,[14] but interfering spinel formation was not observed in that case.

SEM−EDX analysis was performed in the analytical laboratories of Albemarle Catalysts BV. Samples were embedded in Castoglas and polished on SiC paper with 2-propanol. Samples were then carbon-coated to improve conductivity and line-scans were recorded across the cross-section of a bisected pellet with a step size of 10 μm at a 20-kV acceleration voltage.

Results and Discussion

1. Drying Phenomena inside γ-Al_2O_3 Pellets after Impregnation with Co/Mo/P/Citric Acid Solutions. *Chemistry of Phosphomolybdocobaltate Solutions.* Solutions containing molybdate and phosphate are known to host a multitude of phosphomolybdate species in acidic aqueous environment.[11] In the presence of cobalt the phosphomolybdocobaltate heteropolyanion $H_xPMo_{11}CoO_{40}^{(7-x)-}$, which is the complex of interest in this study, is formed at certain P/Mo ratios (and pH values), see eq 1.

$$11H_xMo_7O_{24}^{(6-x)-} + 7H_xPO_4^{(3-x)-} + 7[Co(OH_2)_6]^{2+} \rightleftarrows 7H_xPMo_{11}CoO_{40}^{(7-x)-} \quad (1)$$

The different species present in the Co/Mo/P solutions as a function of the H_3PO_4 concentration have been investigated in a titration experiment where Raman and UV−vis spectroscopy were used to identify the different species.[14] These experimental results show that $PMo_{11}Co$ is the predominant species in the range of $0.08 < P/Mo < 0.20$, which is in agreement with calculations based on known equilibrium constants.[14,18] The optimum P/Mo ratio for $PMo_{11}Co$ was found to be 0.12, in which case 88% of all Mo is present in the complex.[14] Upon decreasing the P/Mo ratio from 0.12 onward, increasing amounts of $H_xMo_7O_{24}^{(6-x)-}$ are observed; however, at higher P/Mo ratios, $H_xP_2Mo_5O_{23}^{(6-x)-}$ (abbreviated as P_2Mo_5) becomes the predominant species. The Raman and UV−vis−NIR spectra of the CoMoP(0.12) solution are depicted in Figure 2, parts a and b, respectively. The $PMo_{11}Co$ complex is characterized by Raman bands at 971 (with a shoulder at 954 cm^{-1}), 886, and 228 cm^{-1} and by bands at 17600 (Co^{2+} $d-d$ transition) and 22000 cm^{-1} ($O \rightarrow Mo^{6+}$ charge-transfer band) in the UV−vis−NIR spectrum.[14,19] In all UV−vis−NIR spectra, an additional band at 19300 cm^{-1} due to the Co^{2+} hexaaqua complex $[Co(OH_2)_6]^{2+}$ is visible as there is an excess Co^{2+} with respect to $PMo_{11}Co$ in all cases.

Effect of Drying on $PMo_{11}Co$ Distribution inside γ-Al_2O_3 Pellets. After impregnation of γ-Al_2O_3 pellets with a CoMoCAP(0.7) solution and aging for 4 h, $PMo_{11}Co$ is observed only near the center of the γ-Al_2O_3 pellets, as can be concluded from both the Raman and the UV−vis−NIR spectra recorded along the cross-section of a bisected pellet, see Figure 3, parts a and c. The presence of $PMo_{11}Co$ in those positions is evidenced by the Raman band at 971 cm^{-1} and the $O \rightarrow Mo^{6+}$ charge-transfer band at 22000 cm^{-1} in the UV−vis−NIR spectra. After fast drying of this sample after 4-h aging, a reversed $PMo_{11}Co$ gradient is observed, see Figure 3, parts b and d, for the corresponding Raman and UV−vis−NIR spectra. Both the Raman peak at 971 cm^{-1} and charge-transfer band at 22000 cm^{-1} in the UV−vis−NIR spectra indicate the presence of $PMo_{11}Co$ only near the edge of the γ-Al_2O_3 particle after drying. To understand the different $PMo_{11}Co$ distribution before and after drying, we need to consider the migration rates of the different components of which the $PMo_{11}Co$ complex is constituted (eq 1): $[Co(OH_2)_6]^{2+}$ migrates fast into the γ-Al_2O_3 pellets as this positively charged complex has no electrostatic interaction with the surface hydroxyl groups of the support, which are also positively charged at the low pH of the impregnation solution. The transport of molybdate species, on the other hand, is known to occur somewhat more slowly (1−3 h for a homogeneous Mo distribution over the Al_2O_3 support[16]) due to Coulombic interactions with the support. Most importantly, the transport of phosphate is even slower, due to a strong interaction with Al_2O_3:[11]

$$Al_sOH + HPO_4^{2-} + H^+ \rightleftarrows Al_sHPO_4^- + H_2O \quad (2)$$

First of all, the formation of this type of "surface aluminum phosphate" occurs slowly, and thus the amount of free phosphate that stays available for $PMo_{11}Co$ formation decreases slowly. Second, the migration of the free phosphate occurs very slowly;

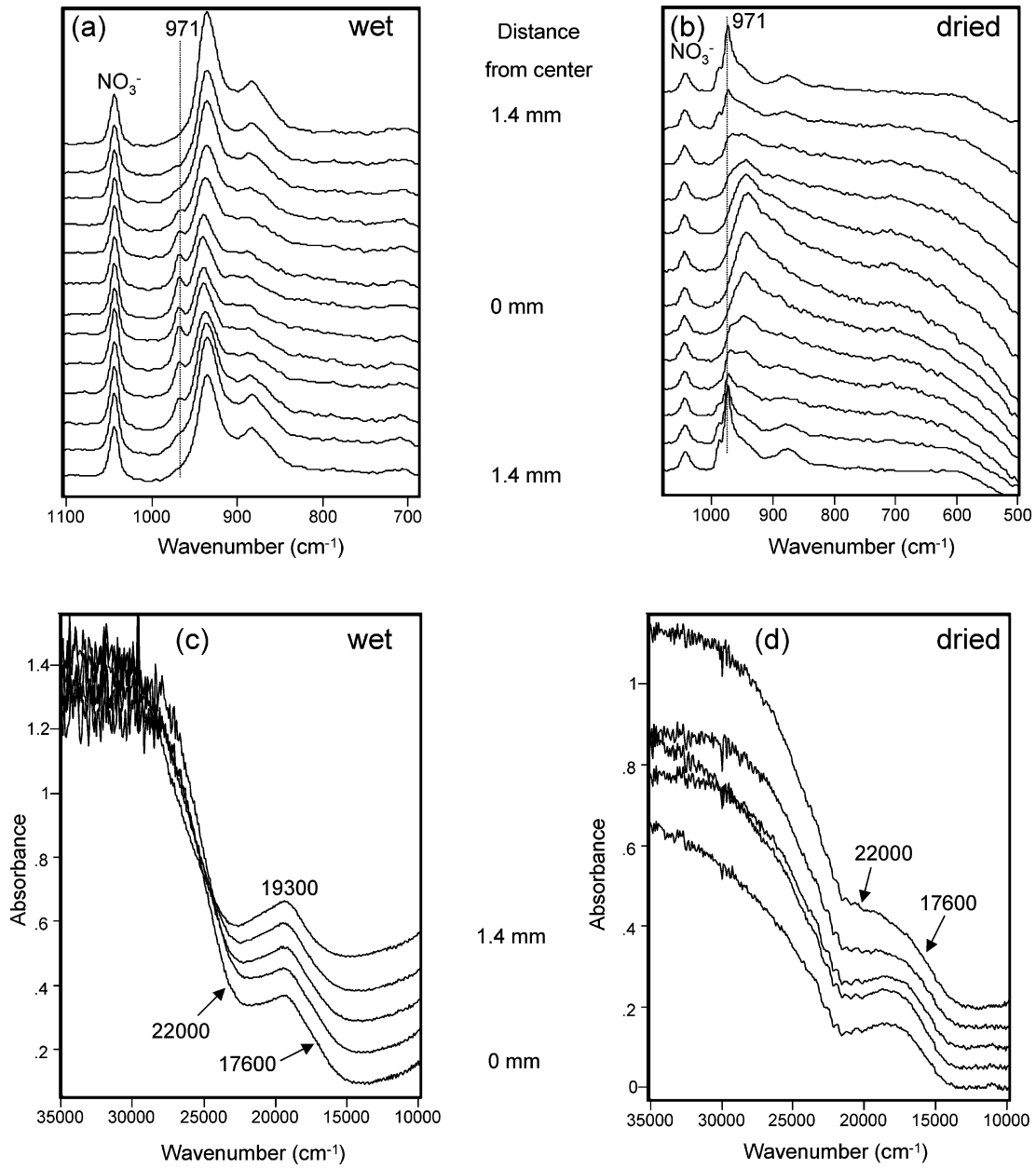

Figure 3. Raman (a and b) and UV−vis−NIR (c and d) line scans across the surface of a bisected pellet showing the distribution profile of $PMo_{11}Co$ in a wet CoMoCAP(0.7) sample after 4-h aging (a and c) and after fast drying of an aged (4-h) CoMoCAP(0.7) sample (b and d). The Raman band indicative of $PMo_{11}Co$ at 971 cm^{-1} is indicated with a dashed line. UV−vis−NIR bands of $PMo_{11}Co$ at 17600 and 22000 cm^{-1} are indicated.

at 4 h after impregnation, that is, at the moment that the samples described here were subjected to drying, no homogeneous phosphate distribution over the pellets has been established yet.[14] At 24 h after impregnation, the phosphate distribution over the catalyst support bodies has been found to be close to homogeneous,[14] which implies that eq 2 is a reversible reaction. The result of this phosphate−support interaction is that a gradient in the free-phosphate concentration over the support bodies is observed, and this is the key to understanding the $PMo_{11}Co$ profiles over the support bodies.

As discussed in the previous section, $PMo_{11}Co$ will be the predominant species in those places where the P/Mo ratio falls in the 0.08−0.20 range. Due to the free-phosphate gradient after 4 h (and the homogeneous Mo distribution at this point in time), a gradient in the P/Mo ratio will be present over the γ-Al_2O_3 pellets. The P/Mo ratio inside γ-Al_2O_3 pellets is defined as the ratio between free phosphate and free Mo, that is, the ratio of available P and Mo for $PMo_{11}Co$ formation (the fraction P that is incorporated in the surface aluminum phosphate is not available for $PMo_{11}Co$ formation). After drying of an aged (4-h) sample, the P/Mo gradient may still exist; however, due to extended reaction of phosphate with the surface according to eq 2, less free phosphate is present and thus the P/Mo ratio is expected to be lower than before drying throughout the whole pellet. Consequently, the positions throughout the Al_2O_3 pellet where the P/Mo ratio is in the optimal range for $PMo_{11}Co$ formation may change upon drying. In Figure 4 the effect of changes in the P/Mo ratio on the $PMo_{11}Co$ distribution are illustrated, where the gray region corresponds to the P/Mo range at which $PMo_{11}Co$ may be observed. The lines drawn in the figure show how the P/Mo gradient over the pellet changes upon drying: due to the lowering of the line upon drying (by sustained reaction of phosphate with the Al_2O_3 surface), different parts of the pellet have the appropriate P/Mo ratio to allow PMo_{11}-

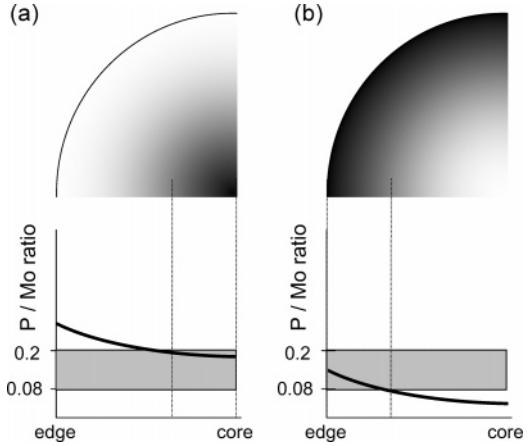

Figure 4. The effect of changes in the P/Mo ratio on the $PMo_{11}Co$ distribution along the cross-section of a bisected γ-Al_2O_3 pellet, impregnated with a CoMoCAP(0.7) solution and aged for 4 h (a) before drying and (b) after fast drying. The gray area in the graph illustrates the P/Mo range where $PMo_{11}Co$ formation is possible. Note that the P/Mo ratio refers to the free phosphate-to-Mo ratio.

Co formation. Before drying, the $H_xPO_4^{(3-x)-}$ concentration near the edge is too high for $PMo_{11}Co$ to be stable, and P_2Mo_5 is indeed the observed species.[14] After drying, the P/Mo ratio near the edge of the sample is expected to be in the 0.08−0.20 range, while the $H_xPO_4^{(3-x)-}$ concentration in the core of the pellets has become too low to render $PMo_{11}Co$ stable. In those positions, a broad band at 930−950 cm^{-1} (Figure 3b), due to polymolybdate ($Mo_xO_y^{z-}$) species,[7] is observed. Alternatively, it might be suggested that an Anderson-type hexamolybdoaluminate $Al(OH)_6Mo_6O_{18}^{3-}$ ($AlMo_6$) is present at positions with a low P/Mo ratio. $AlMo_6$ formation is known to occur upon aging after impregnation of γ-Al_2O_3 with molybdate solutions in the absence of phosphate, where γ-Al_2O_3 is partially dissolved and Al^{3+} is incorporated into the heteropolymolybdate structure.[5c] The Raman bands of $AlMo_6$ are found at 943, 898, and 565 cm^{-1},[5c] but the absence of a band at 565 cm^{-1} (a band that is not found in the spectrum of $Mo_xO_y^{z-}$) in Figure 3b excludes the possibility of $AlMo_6$ formation in this case.

The reaction of phosphate with the alumina surface may have an effect on the pH of the impregnation solution (with initial pH values in the range 1.0−1.2)[14] inside the pellet after aging and drying. Although the change in pH inside the pellet after impregnation is not exactly known, it is unlikely that a large pH increase occurs, since this would lead to depolymerization of the polymolybdates to, for example, MoO_4^{2-}, which displays Raman bands at 896 and 836 cm^{-1}.[16] These bands have not been observed in the Raman spectra recorded on wet pellets

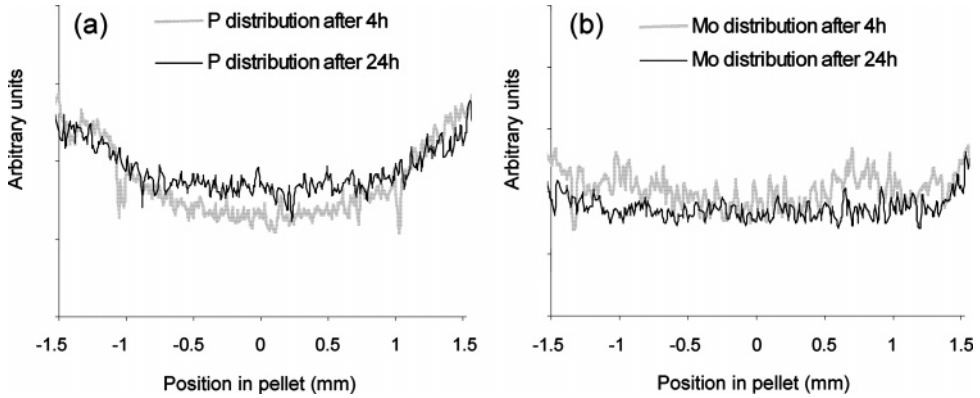

Figure 5. SEM−EDX (a) P and (b) Mo distribution over γ-Al_2O_3 pellets, impregnated with CoMoCAP(0.7), aged for either 4 or 24 h, and dried fast.

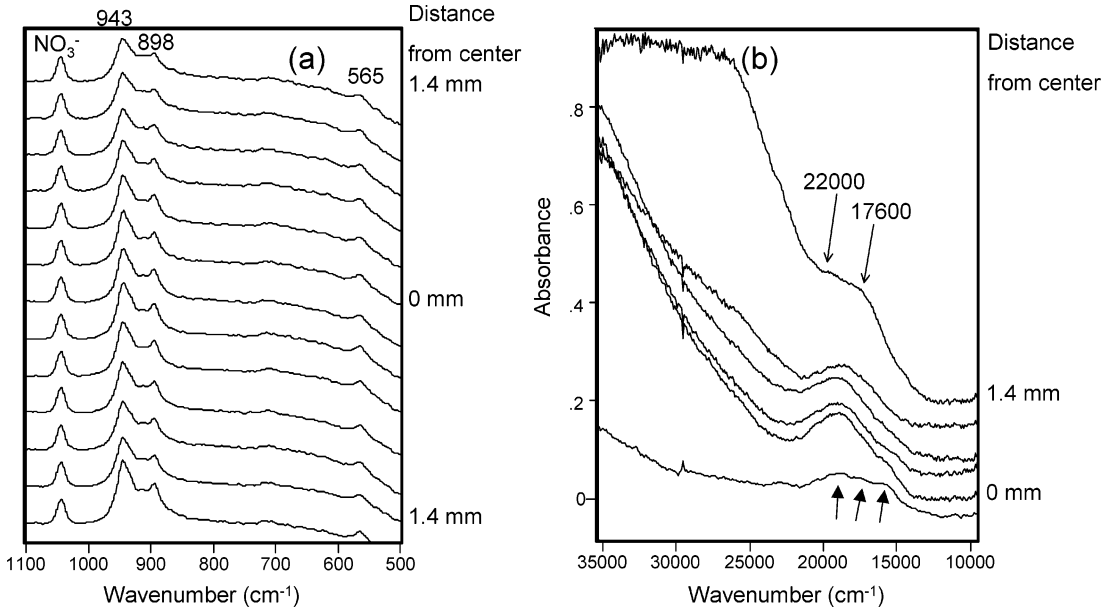

Figure 6. Raman (a) and UV−vis−NIR spectra (b) recorded at different positions inside γ-Al_2O_3 pellets, impregnated with a CoMoCAP(0.3) solution, after 4-h aging and slow drying. The bottom spectrum of Figure 6b is the reference spectrum of $CoAl_2O_4$ spinel, with bands at 15750, 17250, and 19000 cm^{-1}, indicated with arrows.

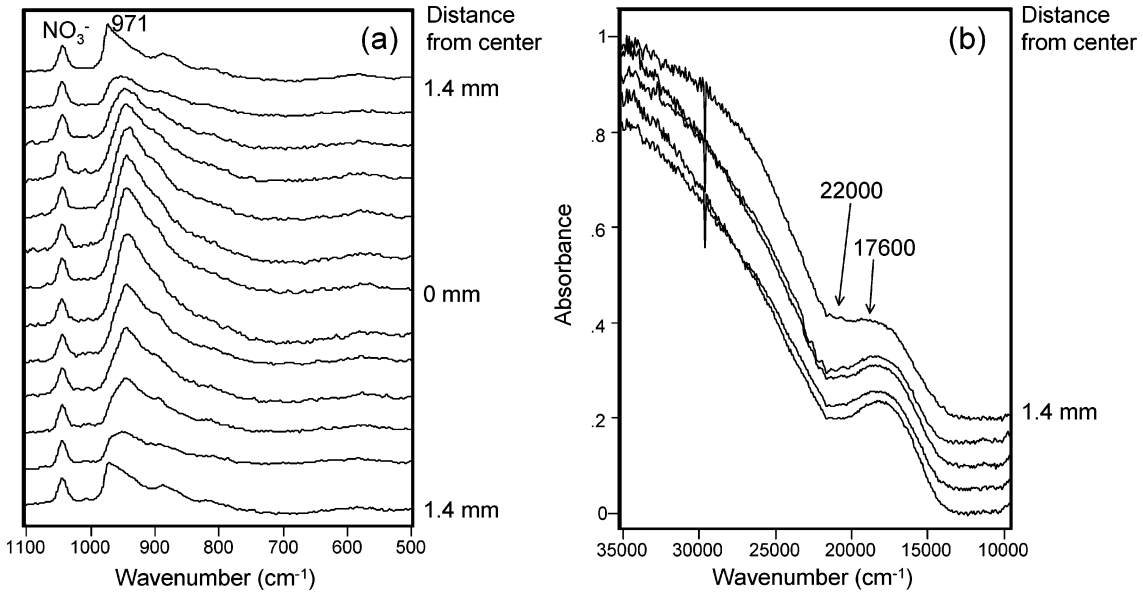

Figure 7. Raman (a) and UV−vis−NIR spectra (b) recorded at different positions inside γ-Al_2O_3 pellets, impregnated with a CoMoCAP(0.3) solution, after 4-h aging and fast drying.

after aging,[14] nor on pellets measured after drying (Figure 3b). Instead, a broad band in the 940−950 cm^{-1} region has been observed, typical of (hetero)polymolybdate species which are stable in acidic environment only.

The distribution of P and Mo over γ-Al_2O_3 bodies after drying was measured with SEM−EDX as a local probing technique. Freshly cut, dried γ-Al_2O_3 pellets, which had been impregnated with a CoMoCAP(0.7) solution and aged for either 4 or 24 h, were analyzed along their cross-sections and the overall Mo and P distributions are presented in Figure 5. The data confirm the assumptions that Mo is homogeneously distributed over the pellet after 4 h, and that the P distribution is not yet at equilibrium after such an aging time. Thus, the P/Mo profiles over dried pellets, as presented in Figure 4, can be safely used to explain the spectroscopic data.

Influence of Drying Rate on $PMo_{11}Co$ Distribution inside γ-Al_2O_3 Pellets. The effect of the drying rate on the final $PMo_{11}Co$ distribution is illustrated for samples impregnated with a CoMoCAP(0.3) solution that were dried after 4-h aging. Prior to drying, a homogeneous distribution of $PMo_{11}Co$ over the wet pellets is observed, with approximately 45% of all Mo present in the complex.[14] The Raman and UV−vis−NIR spectra of the corresponding sample, recorded after 4-h aging and slow drying, are presented in Figure 6. The band indicative of $PMo_{11}Co$ at 971 cm^{-1} has completely disappeared throughout the whole pellet in favor of bands at 943, 898, and 565 cm^{-1}, indicating the presence of $AlMo_6$.[5c] As $AlMo_6$ formation occurs in the absence of $H_xPO_4^{(3-x)-}$, we conclude that $PMo_{11}Co$ decomposition results from the decreased $H_xPO_4^{(3-x)-}$ concentration upon drying due to reaction with the support according to eqs 1 and 2, as described in the previous section. The Raman spectra recorded after fast drying are significantly different from those after slow drying, see Figure 7a. Near the edges of the cross-section, the 971 cm^{-1} band of $PMo_{11}Co$ is still visible. Second, the bands due to $AlMo_6$ at 943, 898, and 565 cm^{-1} are not observed; instead a broad band at 945 cm^{-1} has emerged which is probably due to adsorbed polymolybdate species.[5c] Apparently, $AlMo_6$ formation occurs only at elevated temperatures in combination with the presence of some residual water, that is, upon slow drying.

The UV−vis−NIR spectra are in agreement with the Raman spectra. The disproportionation of $PMo_{11}Co$ upon drying is evident, especially so after slow drying, see Figures 6b and 7b. At the exterior of the analyzed catalyst bodies, a small amount of $PMo_{11}Co$ is still present, as can be concluded from the $O \rightarrow Mo^{6+}$ charge-transfer band at 22000 cm^{-1} and the Co^{2+} $d-d$ transition band at 17600 cm^{-1}. Inside the pellets, Co^{2+} is mainly present as $[Co(OH_2)_6]^{2+}$, which is identifiable by an absorption at 19300 cm^{-1}. The second conclusion that can be drawn from the UV−vis−NIR spectra is that a $CoAl_2O_4$ spinel phase has been formed after slow drying, as indicated by a band at 15750 cm^{-1}, which is not visible in the spectra in Figure 7b. Evidence for this assignment has been provided by a reference spectrum of the $CoAl_2O_4$ phase, obtained after drying of an Al_2O_3 sample that was impregnated with $Co(NO_3)_2$, see the bottom spectrum in Figure 6b. The observed bands at 15750, 17250, and 19000 cm^{-1} are in agreement with observations by Papadopoulou et al.[5e]

The second example that illustrates the effect of the drying rate on the $PMo_{11}Co$ distribution is provided by a sample impregnated with CoMoCAP(1.5) which was aged for 4 h. After slow drying of this sample, a homogeneously distributed small amount of $PMo_{11}Co$ is observed, as indicated by the Raman band at 971 cm^{-1}, see Figure 8a. After fast drying of the same sample, a substantial amount of $PMo_{11}Co$ is found near the center of the γ-Al_2O_3 pellets, see Figure 8b. The differences caused by the different drying rate can be explained by assuming that there is still a small amount of water present at the early stages of the slow drying process. The combination of this residual water with the slightly elevated temperature allows the reaction of phosphate with the surface to continue (eq 2) and, second, allows the phosphate migration to continue at the beginning of the slow drying process. As a result, the concentration of free phosphate is expected to be slightly lower, and more uniformly distributed, upon slow drying. The result is that upon slow drying of a sample that was impregnated with CoMoCAP-(0.3), the phosphate concentration throughout the whole sample has become too low to allow $PMo_{11}Co$ formation. On the contrary, upon fast drying the P/Mo ratio near the edge of the sample may be just high enough to be in the region where $PMo_{11}Co$ can still be formed. In Figure 9a, a visualization of this effect is given for the CoMoCAP(0.3) case. In the case of CoMoCAP(1.5), the phosphate concentration after 4-h aging in the core of the pellet is still low enough to allow $PMo_{11}Co$

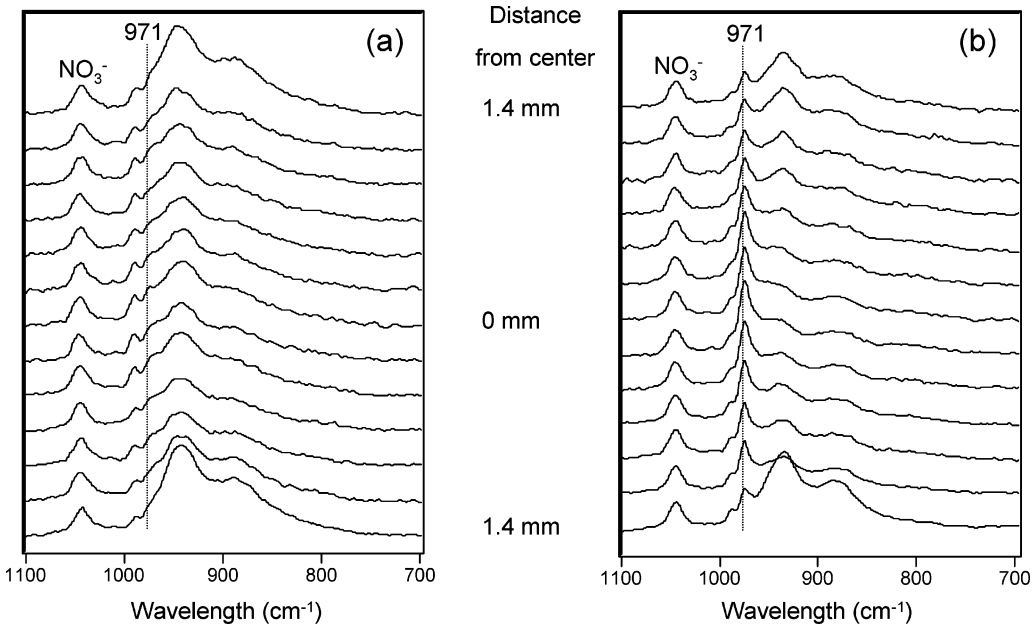

Figure 8. Raman spectra recorded at different positions inside γ-Al_2O_3 pellets, impregnated with a CoMoCAP(1.5) solution, after 4-h aging and slow (a) or fast (b) drying.

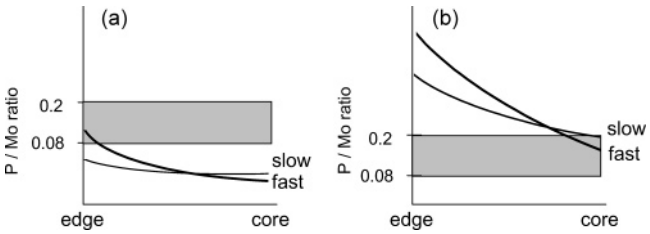

Figure 9. Schematic representation of the effect of the drying rate on the observed $PMo_{11}Co$ distribution. Samples were impregnated with (a) CoMoCAP(0.3) or (b) CoMoCAP(1.5) solutions.

formation; after fast drying the P/Mo ratio is therefore still below 0.20 in these positions. After slow drying, however, a high phosphate concentration has been established throughout the whole pellet due to enhanced phosphate migration toward the core, which is not compensated by a drop in free-phosphate concentration due to extended reaction with the Al_2O_3 surface (even in the core of the pellets the P/Mo ratio is higher than 0.20). After slow drying, P_2Mo_5 rather than $PMo_{11}Co$ is observed throughout the whole pellet, see Figure 9b.

Influence of the Initial Phosphate Concentration on the $PMo_{11}Co$ Distribution Profile. In the previous sections, both an egg-shell and an egg-yolk distribution of $PMo_{11}Co$ over γ-Al_2O_3 have been obtained, either by fast drying of a CoMoCAP(0.7) or CoMoCAP(0.3) sample after 4-h aging (egg-shell) or by fast drying of a CoMoCAP(1.5) after 4-h aging (egg-yolk). To obtain a homogeneous distribution of $PMo_{11}Co$ after drying, the P/Mo ratio needs to be in the 0.08−0.20 range throughout the whole sample. Indeed, when applying a CoMoCAP(1.0) solution for the impregnation, aging the sample for 4 h and drying the sample at a fast rate, a homogeneous $PMo_{11}Co$ distribution over the pellets has been achieved, see Figure 10 for the Raman spectra across a bisected pellet. These results show that, by applying the right conditions during impregnation and drying, the distribution of the catalyst precursor $PMo_{11}Co$ after drying can be successfully determined.

2. Quantitative Analysis of Raman Data. The spectroscopic results presented here have been considered in a qualitative way only so far. We have made an attempt to evaluate the data in a more quantitative way. As the method of choice, a reference

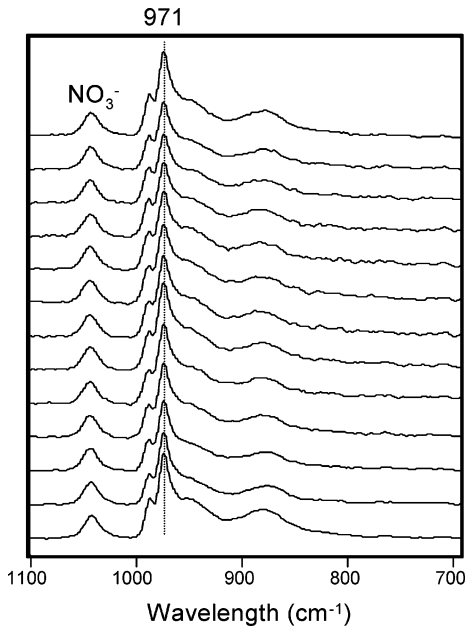

Figure 10. A homogeneous $PMo_{11}Co$ distribution inside a γ-Al_2O_3 sample obtained after impregnation with a CoMoCAP(1.0) solution, 4-h aging, and fast drying.

spectrum recorded from a sample with a known $PMo_{11}Co$ concentration has been applied. To obtain such a γ-Al_2O_3 sample with a $PMo_{11}Co$ concentration as high as possible after drying, a range of drying experiments on crushed γ-Al_2O_3 pellets have been performed. Impregnations were carried out with crushed γ-Al_2O_3 bodies (150−500-μm sieve fraction) and CoMoCAP-(x) solutions with x ranging from 0.3 to 2.0 M. The Raman and UV−vis−NIR spectra of these powders, recorded after aging (4 h) and fast drying, are depicted in Figure 11, parts a and b, respectively. The Raman spectra in Figure 11a show that the $PMo_{11}Co$ complex is present in all samples; the optimum H_3PO_4 concentration for the formation of this complex upon aging and drying appears to be around 0.8 M. This value for the optimum (in terms of $PMo_{11}Co$ formation) H_3PO_4 concentration suggests that the free-phosphate concentration in the system has decreased in such a way that a P/Mo (where P is free phosphate)

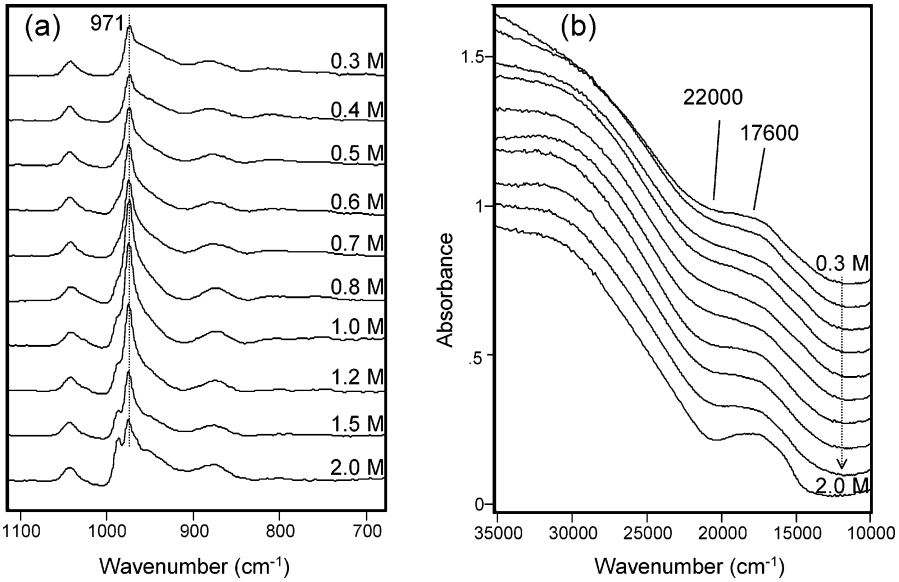

Figure 11. (a) Raman and (b) UV−vis−NIR spectra showing the presence of $PMo_{11}Co$ on crushed γ-Al_2O_3 pellets after impregnation, 4-h aging, and fast drying, as a function of H_3PO_4 concentration x in the CoMoCAP(x) impregnation solution.

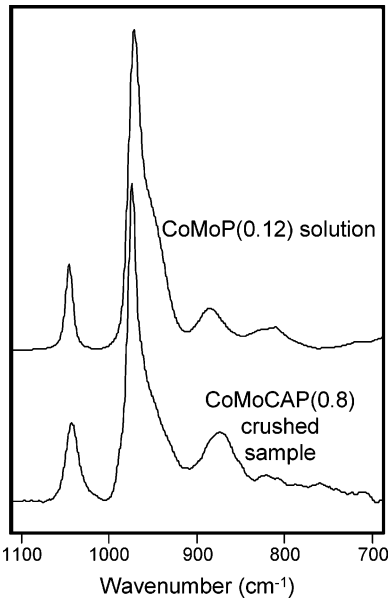

Figure 12. Comparison of the Raman spectra of CoMoCAP(0.12) (solution) and CoMoCAP(0.8) (crushed sample).

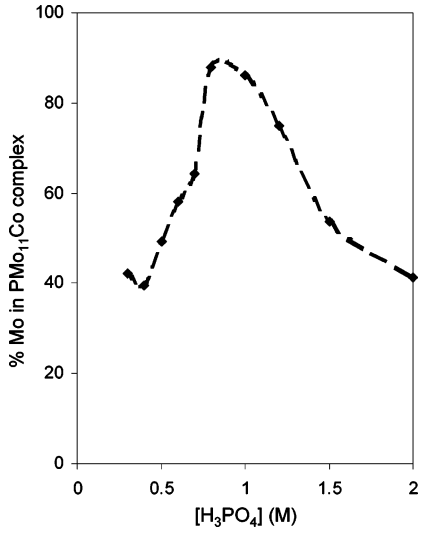

Figure 13. Relative amount of Mo present in $PMo_{11}Co$ in the different CoMoCAP(x) powder samples, based on the relative peak heights of the Raman band at 971 cm^{-1}. Spectra have been normalized to the NO_3^- peak.

ratio of around 0.12 is obtained after an aging time of 4 h and the applied drying procedure, according to the same mechanism of reaction of phosphate with the Al_2O_3 surface (eq 2) as described earlier. In cases where the initial H_3PO_4 concentration in the solution was lower than 0.8 M, a shoulder next to the 971-cm^{-1} peak at lower wavenumber is observed, characteristic of polymolybdate species on alumina.[7] These observations support the idea that decomposition of $PMo_{11}Co$ on γ-Al_2O_3 occurs upon aging and drying when solutions with low initial H_3PO_4 concentrations are applied. Samples prepared from solutions with higher H_3PO_4 levels (CoMoCAP(x) solutions with $x > 0.8$) show additional Raman bands due to phosphomolybdate species such as PMo_9 or PMo_{11} at around 965 cm^{-1}, and PMo_{12} at 987 cm^{-1}, according to Van Veen et al.[11] In these cases, Co is removed from the $PMo_{11}Co$ complex and is present either as the hexaaqua complex $[Co(OH_2)_6]^{2+}$, in a complex with citrate, $[Co(citrate)_2]$, or it may react with the Al_2O_3 surface to form $CoAl_2O_4$ surface spinel. Close inspection of the UV−vis−NIR spectra of the dried impregnated powders of samples with $x > 1.0$ (Figure 11b) reveals the presence of a minor shoulder at 15750 cm^{-1}, indicative of some $CoAl_2O_4$.

As the Raman spectrum of the CoMoCAP(0.8) powder sample, recorded after aging and drying, has the highest PMo_{11}-Co content, this spectrum was selected for the quantification. In Figure 12, this spectrum is compared with the spectrum of a CoMoP(0.12) solution, where small differences in the peak positions are due to the fact that one spectrum was recorded from a solution and the second from a solid sample. The high similarity of these spectra prompted us to assume that in the CoMoCAP(0.8) powder sample the same fraction of the Mo (i.e., 88%) as in the CoMoP(0.12) solution sample is accommodated in $PMo_{11}Co$, and this value of 88% Mo in $PMo_{11}Co$ in the reference spectrum will thus be used. The relative amounts of $PMo_{11}Co$ in the different powder samples are compared in Figure 13.

The spectra recorded from bisected pellets have been baseline-corrected and subsequently scaled at the NO_3^- peak at 1048 cm^{-1}. Semiquantitative values of the % Mo in $PMo_{11}Co$ at

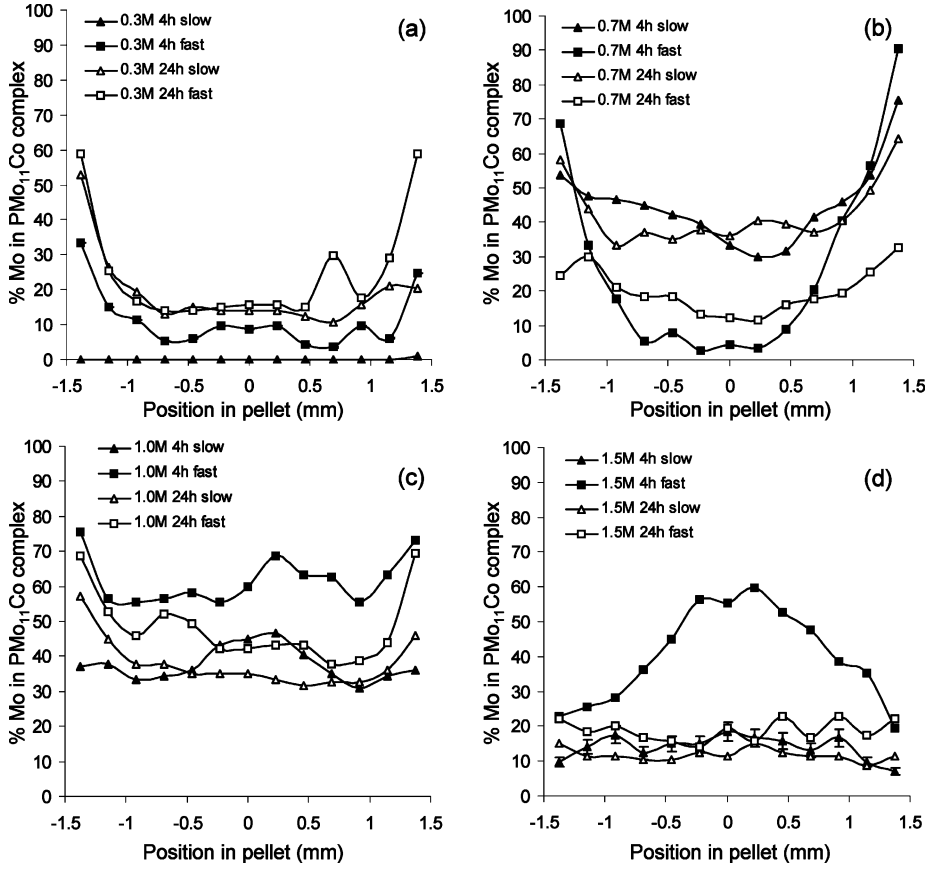

Figure 14. Relative amounts of Mo in $PMo_{11}Co$ after impregnation with CoMoCAP(x) solutions with $x = 0.3$ (a), 0.7 (b), 1.0 (c), and 1.5 (d) after 4-h or 24-h aging and either slow or fast drying. The relative error in the data is estimated to be approximately 15%.

different positions in the samples are obtained by subtraction of each spectrum with the 88% reference spectrum. The accuracy of these values is limited, mainly because the amount of $PMo_{11}Co$ present in the reference spectrum has been deduced by comparing the spectrum of a sample in solution with a spectrum of a solid sample. The overall error in the quantitative data is estimated to be approximately 15%. The quantitative data presented here are helpful in visualizing the results and they allow us to highlight the observed trends in the results. As such, semiquantitative data provide an aid in presenting these data in a concise manner.

An overview of the semiquantitative Raman results of samples analyzed after impregnation with CoMoCAP(x) solutions ($x = 0.3$, 0.7, 1.0, and 1.5), aging for 4 or 24 h, and either slow or fast drying, is presented in Figure 14. The general trend in the results is that a maximum in the $PMo_{11}Co$ content is observed at $x = 1.0$ (Figure 14c). The egg-shell distributions as discussed earlier (CoMoCAP(0.3) and CoMoCAP(0.7), aged 4 h and dried at a fast rate), and the discussed egg-yolk distribution of $PMo_{11}Co$ in the CoMoCAP(1.5) sample (4-h aging, fast drying) are clearly visible in Figure 14, parts a, b, and d, respectively.

The information that can be obtained from the data as presented in Figure 14 will be illustrated by two salient examples. First, the simultaneous influence of both the aging time and the drying rate on the $PMo_{11}Co$ distribution is illustrated clearly in Figure 14d: only after fast drying of a 4-h aged sample is a significant amount of $PMo_{11}Co$ observed in the sample. Changes in either of the variables cause the $PMo_{11}Co$ content to drop below 20% throughout the whole sample. The second example comprises a γ-Al_2O_3 sample, impregnated with a CoMoCAP(0.3) solution (Figure 14a). The $PMo_{11}Co$ content throughout the pellet after 24-h aging and drying is higher than after 4-h aging and drying, irrespective of the applied drying rate, see Figure 14a. This is not in agreement with the rationalization provided to explain the results in the previous sections. In those cases, a decreasing free-phosphate concentration (and thus P/Mo ratio) upon aging and drying has been the explanation for changes in the observed $PMo_{11}Co$ profiles after drying. However, in the case of experiments involving CoMoCAP(0.3) solutions, not only does the $H_xPO_4^{(3-x)-}$ concentration decrease due to reaction with the Al_2O_3 surface. At low $H_xPO_4^{(3-x)-}$ levels, Mo is also known to react with the Al_2O_3 support, yielding the previously discussed Anderson-type $AlMo_6$ complex, identified by a Raman band at 565 cm^{-1} (cf. Figure 6a). When the Mo depletion is more pronounced than the decrease in the $H_xPO_4^{(3-x)-}$ concentration after 24-h instead of 4-h aging, a net increase in the P/Mo ratio may result that is sufficient to allow the formation of (some) $PMo_{11}Co$ after 24 h and drying.

Conclusions

The combination of two spatially resolved spectroscopic techniques allows a good understanding of the physicochemical processes occurring inside catalyst−support bodies during the first stages of the preparation process. Studying the preparation process of supported catalyst bodies reveals information that cannot be obtained by studying powdered samples. The formation and decomposition of the $PMo_{11}Co$ complex, which is anticipated to be an interesting precursor for $CoMoS_2/\gamma$-Al_2O_3 catalysts, inside Al_2O_3 pellets has been related to variations in the local P/Mo ratios (where P refers to the free-phosphate concentration), the value of which should be in the 0.08−0.20 range for $PMo_{11}Co$ to be stable. These variations in the P/Mo ratios are caused by differences in migration rate of P, Mo, and

Co inside the support bodies. The slow migration rate of phosphate is due to strong interactions with the Al_2O_3 surface according to eq 2. This reaction with Al_2O_3 takes place from the start of the impregnation and continues until the last traces of water have been removed from the sample during the drying process. The effect of the drying rate on the $PMo_{11}Co$ distribution after drying supports this idea, as traces of water are still present during the first stage of the slow drying process. By varying the composition of the impregnation solution, the aging time, and the drying procedure, either a homogeneous, an egg-shell, or an egg-yolk distribution of the $PMo_{11}Co$ complex may be obtained after drying. Impregnation and drying experiments involving powdered γ-Al_2O_3 support bodies proved to be useful for obtaining a reference spectrum of $PMo_{11}Co$ on Al_2O_3, which has been used for the quantification of the Raman results.

The Raman and UV−vis−NIR microspectroscopy techniques described here are of great value in understanding the preparation process of heterogeneous catalysts. Raman microscopy can be used to study catalytic systems that contain (transition) metal species with Raman active M−O vibrations. UV−vis−NIR microspectroscopy may prove useful in studying both charge-transfer bands and $d-d$ transitions of (transition) metal species inside catalyst supports. This better understanding of the catalyst preparation process is expected to be beneficial for the development of catalysts with improved properties.

References and Notes

(1) (a) Bell, A. T. *Science* **2003**, *299*, 1688−1691. (b) de Jong, K. P. *CatTech* **1998**, *3*, 87−95. (c) *Handbook of Heterogeneous Catalysis*, Vol. 1; Ertl, G., Knözinger, H., Weitkamp, J., Eds.;Wiley-VCH: Weinheim, 1997.

(2) Schlögl, R.; Abd Hamid, S. B. *Angew. Chem., Int. Ed.* **2004**, *43*, 1628−1637.

(3) (a) Neimark, A. V.; Kheifez, L. I.; Fenelonov, V. B. *Ind. Eng. Chem. Prod. Res. Dev.* **1981**, *20*, 439−450. (b) Lekhal, A.; Glasser, B. J.; Khinast, J. G. *Chem. Eng. Sci.* **2004**, *59*, 1063−1077.

(4) Topsøe, H.; Clausen, B. S.; Candia, R.; Wivel, C.; Morup, S. *J. Catal.* **1981**, *68*, 433−452.

(5) (a) Cattaneo, R.; Shido, T.; Prins, R. *J. Catal.* **1999**, *185*, 199−212. (b) Kraus, H.; Prins, R. *J. Catal.* **1997**, *170*, 20−28. (c) Carrier, X.; Lambert, J. F.; Kuba, S.; Knözinger, H.; Che, M. *J. Mol. Struct.* **2003**, *656*, 231−238. (d) Grange, P.; Vanhaeren, X. *Catal. Today* **1997**, *36*, 375−391. (e) Papadopoulou, Ch.; Vakros, J.; Matralis, H. K.; Kordulis, Ch.; Lycourghiotis, A. *J. Colloid Interface Sci.* **2003**, *261*, 146−153. (f) Heinerman, J. J. L.; van Hengstum, A. J.; de Wind, M. Eur. Pat. 469,675, 1991.

(6) Jongsomjit, B.; Panpranot, J.; Goodwin, J. G., Jr. *J. Catal.* **2001**, *204*, 98−109.

(7) (a) Carrier, X.; Lambert, J. F.; Che, M. *J. Am. Chem. Soc.* **1997**, *119*, 10137−10146. (b) Le Bihan, L.; Blanchard, P.; Fournier, M.; Grimblot, J.; Payen, E. *J. Chem. Soc., Faraday Trans.* **1998**, *94*, 937−940.

(8) Martin, C.; Lamonier, C.; Fournier, M.; Mentré, O.; Harlé, V.; Guillaume, D.; Payen, E. *Inorg. Chem.* **2004**, *43*, 4636−4644.

(9) Cabello, C. I.; Botto, I. L.; Thomas, H. J. *Appl. Catal. A: General* **2000**, *197*, 79−86.

(10) (a) Griboval, A.; Blanchard, P.; Payen, E.; Fournier, M.; Dubois, J. L.; Bernard, J. R. *Appl. Catal. A: General* **2001**, *217*, 173−183. (b) Griboval, A.; Blanchard, P.; Gengembre, L.; Payen, E.; Dubois, J. L.; Bernard, J. R. *J. Catal.* **1999**, *188*, 102−110. (c) Griboval, A.; Blanchard, P.; Payen, E.; Fournier, M.; Dubois, J. L. *Catal. Today* **1998**, *45*, 277−283.

(11) van Veen, J. A. R.; Hendriks, P. A. J. M.; Andréa, R. R.; Romers, E. J. G. M.; Wilson, A. E. *J. Phys. Chem.* **1990**, *94*, 5282−5285.

(12) Vázquez, P. G.; González, M. G.; Blanco, M. N.; Cáceres, C. V. *Stud. Surf. Sci. Catal.* **1995**, *91*, 1121−1130.

(13) (a) Combs-Walker, L. A.; Hill, C. L. *Inorg. Chem.* **1991**, *30*, 4016−4026. (b) Matsumoto, Y.; Asami, M.; Hashimoto, M.; Misono, M. *J. Mol. Catal. A: Chemical* **1996**, *114*, 161−168.

(14) Bergwerff, J. A.; van de Water, L. G. A.; Visser, T.; Leliveld, R. G.; de Jong, K. P.; Weckhuysen, B. M. *Chem. Eur. J.*, in press.

(15) van de Water, L. G. A.; Bergwerff, J. A.; Nijhuis, T. A.; de Jong, K. P.; Weckhuysen, B. M. *J. Am. Chem. Soc.* **2005**, *127*, 5024−5025.

(16) Bergwerff, J. A.; Visser, T.; Leliveld, B. R. G.; Rossenaar, B. D.; de Jong, K. P.; Weckhuysen, B. M. *J. Am. Chem. Soc.* **2004**, *126*, 14548−14556.

(17) Simpson, H. D.; Borgens, P. B. Eur. Pat. 0 341 893, 1989.

(18) (a) Cruywagen, J. J.; Rohwer, E. A.; Wessles, G. F. S. *Polyhedron* **1995**, *14*, 3481−3493. (b) Petterson, L.; Andersson, I.; Öhman, L. O. *Inorg. Chem.* **1986**, *25*, 4726−4733. (c) Leyrie, M.; Fournier, M.; Massart, R. *C. R. Acad. Sci. Sér. C* **1971**, *273*, 1569−1572.

(19) Griboval, A.; Blanchard, P.; Payen, E.; Fournier, M.; Dubois, J. L.; Bernard, J. R. *Stud. Surf. Sci. Catal.* **1999**, *127*, 361−364.